Hyperbolic Heat Conduction with Convection Boundary Conditions and Pulse Heating Effects

David E. Glass*
Analytical Services & Materials, Hampton, Virginia 23666
and
Kumar K. Tamma† and Sudhir B. Railkar‡
University of Minnesota, Minneapolis, Minnesota 55455

This paper describes the numerical simulation of hyperbolic heat conduction with convection boundary conditions. The effect of a step heat loading, a sudden pulse heat loading, and a pulse internal heat source are considered in conjunction with convection boundary conditions. Two methods of solution are presented for predicting the transient behavior of the propagating thermal disturbances. In the first method, MacCormack's predictor-corrector method is employed for integrating the hyperbolic system of equations. Next the transfinite element method, which employs specially tailored elements, is used for accurately representing the transient response of the propagating thermal wavefronts. The agreement between the results of various numerical test cases not only validates the representative behavior of the thermal wave fronts but also provides an understanding of the representative behavior due to convection boundary conditions and varied heating effects.

Nomenclature

A = array defined by Eq. (5e)
a_n = arbitrary constant
Bi = Biot number, $= hL/k_r$
C = dimensionless specific heat, $= c_p/c_{pr}$
c_j = arbitrary constant
c_p = constant pressure specific heat
c_{pr} = reference constant pressure specific heat
E = vector defined by Eq. (5b)
e = enthalpy
F = vector defined by Eq. (5c)
G = dimensionless internal heat generation, $= 4gL^2/k_rT_r$
g = internal heat generation
H = dimensionless enthalpy, $H = e/(\rho_r c_{pr} T_r)$
h = heat-transfer coefficient
K = dimensionless thermal conductivity, $= k/k_r$
$\bar{K}$ = thermal conductance matrix in the transform domain
k = thermal conductivity
k_r = reference thermal conductivity
L = slab half-thickness
$\bar{L}$ = differential operator in transform domain
l_e = element length in transfinite element analysis
N = element thermal interpolation functions
Q = dimensionless heat flux, $= q/q_{abs}$
q = conduction heat flux
R = dimensionless density, $= \rho/\rho_r$
$\bar{R}$ = thermal load vector in the transform domain
S = source term vector defined by Eq. (5d)
s = Laplace transform variable
T = temperature
T_r = reference temperature, $= q_{abs}L/k_r$
t = time
W = weighting functions
x = position
α_r = reference thermal diffusivity
β = defined in Eq. (13f)
$\delta(\xi)$ = dirac delta function
η = dimensionless position, $= x/2L$
θ = dimensionless temperature, $= T/T_r$
$\bar{\theta}$ = temperature vector in the transform domain
λ = defined in Eq. (13e)
ν = Courant number $= \Delta\xi/\Delta\eta$
ξ = dimensionless time, $= \alpha_r t/2L^2$
ρ = density
τ = dimensionless thermal relaxation time, $= \alpha_r \tau'/L^2$
τ' = thermal relaxation time
ϕ = particular solution
$\bar{\Psi}$ = related to initial conditions and load terms
Ω = physical domain

Subscripts
abs = absorbed value at surface
i = spatial node
p = particular solution
r = reference values
∞ = ambient conditions
0 = left surface ($\eta = 0$)
1 = right surface ($\eta = 1$)

Superscripts
$\sim$ = predicted time level
$-$ = transformed domain
$'$ = dummy variable of integration
n = time level in Eq. (6), order of derivative in Eq. (8)

Received May 7, 1989; presented as Paper 89-1683 at the AIAA Thermophysics Conference, Buffalo, NY, June 12-14, 1989; revision received Nov. 29, 1989; second revision received Feb. 7, 1990; accepted for publication Feb. 22, 1990.

*Research Engineer. Member AIAA.
†Associate Professor, Department of Mechanical Engineering. Member AIAA.
‡Graduate Research Assistant, Department of Mechanical Engineering. Member AIAA.

Introduction

THE conduction of heat in solids is usually modeled as a diffusion process in which thermal disturbances propagate with infinite velocities. This classical theory of heat conduction is based on the Fourier heat flux equation, which, being a steady-state equation, does not account for the short time required for the heat flux distribution to be established

when a temperature gradient is suddenly introduced in a solid.[1] Although infinite propagation speeds and an instantaneous steady-state heat flux are not physically accurate, they are acceptable for most engineering applications. However, in some situations, primarily those involving extremely short times or temperatures near absolute zero, the mode of heat conduction is not diffusive (parabolic), but propagative (hyperbolic). There have been numerous observations of thermal waves (second sound) in cryogenic fluids.[2-4] However, due to the short times involved, few experimental data have been presented concerning hyperbolic heat conduction (HHC) above cryogenic temperatures.[5-7] Brorson et al.[5] have observed a heat-transport velocity of approximately 10^8 cm/s in thin gold films upon heating with laser pulses. Though the convergence time between the hyperbolic and parabolic solutions is quite small, the temperature differences between the solutions may be important when temperatures need to be predicted at extremely short times after loading. The approximation of steady-state heat flux and an infinite velocity for the thermal disturbances may then lead to an inaccurate solution. It is in these cases that the parabolic heat conduction equation may be unable to accurately model the heat transfer, and the HHC equation, which allows for a transient heat flux and thus a finite speed of propagation, should be used to model the temperatures in the medium.

The concept of HHC dates back to Maxwell[8] and has since been derived by several different approaches.[9-12] Several analytical and numerical solutions of the HHC equation have been presented in the literature. Maurer and Thompson[13] and Baumeister and Hamill[14] used Laplace transforms to study non-Fourier heat conduction. Özisik and Vick[15] have used integral transforms to study the effect of heat pulses. In addition, Wiggert[16] has used the method of characteristics, Glass et al.[17] have used MacComack's finite-difference method, and Tamma and Railker[18,19] have used the transfinite element method to model/analyze HHC-related problems. Solutions with different boundary conditions have also been studied. Wu[20] and Glass et al.[21] have studied radiation boundary conditions, whereas Glass et al.[22] have numerically studied a periodic surface heat flux.

In the present paper the effects of convection boundary conditions are studied for linear HHC in a slab subjected to a constant step heat flux, a pulse loading situation, or internal heat generation. In the numerical simulation of this class of problems, the major difficulties encountered include spurious oscillatory solution behavior when sharp fronts are involved and defining the sharp discontinuities of the propagating wave front with high resolution. Fundamental results involving convection with various heating effects including the precise determination of the true response of the propagating thermal behavior for HHC models are not available. Hence, the present paper seeks to provide accurate representations of HHC with convection and various pulse loading situations. In particular, the methods used in the analysis are 1) MacCormack's predictor-corrector method (finite-difference approximation) and 2) hybrid transfinite element formulations that combine transform methods and classical Galerkin schemes with finite elements as the principal computational tool. The effects of convective boundary conditions and various thermal loading are herein studied. Several numerical cases are presented that not only provide accurate representations for HHC influenced by convection boundary conditions but also help to understand the representative behavior and mechanisms due to the varied heating effects. In addition, the present work may provide useful information for potential laser applications of short-duration localized heating.

Formulation

The medium was taken to be a slab of dimensionless thickness $\eta = 1$, as shown in Fig. 1. The thermal properties within the medium, as well as the thermal relaxation time, were assumed to be constant. The HHC equation resulting from the use of the non-Fourier heat flux equation is given in dimensionless form as

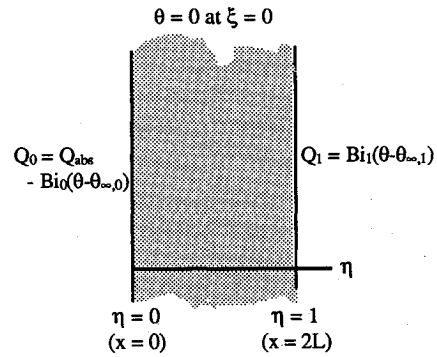

Fig. 1 Hyperbolic heat conduction through a finite slab.

$$\tau \frac{\partial Q}{\partial \xi} + 2Q + K \frac{\partial \theta}{\partial \eta} = 0 \tag{1}$$

The relaxation time τ determines the importance of the non-Fourier terms. If the relaxation time is zero, the HHC equations reduce to the corresponding parabolic model wherein the energy transport is diffusive. As the relaxation time increases, the hyperbolic effects significantly dominate, and the speed of the thermal propagation is reduced. Clearly, when $\tau = 0$, the non-Fourier heat flux equation reduces to the classical Fourier heat flux equation as

$$Q = -\frac{K}{2} \frac{\partial \theta}{\partial \eta} \tag{2}$$

Although the heat flux equations are different for the hyperbolic and parabolic formulations, the energy equation is the same for both formulations and is given in dimensionless form as

$$\frac{\partial \theta}{\partial \xi} + \frac{1}{RC} \frac{\partial Q}{\partial \eta} - \frac{G}{2RC} = 0 \tag{3a}$$

In the finite-difference solution of the hyperbolic problem, the enthalpy formulation is used, and the energy equation takes the form

$$\frac{\partial H}{\partial \xi} + \frac{\partial Q}{\partial \eta} - \frac{G}{2} = 0 \tag{3b}$$

where H is defined as

$$H = \int_0^{\theta} R(\theta')C(\theta')\, d\theta' \tag{3c}$$

and G is of magnitude $1/\Delta\eta$ in the region $0 \le \eta \le \Delta\eta$ at time $\xi = 0$, and is thus taken as

$$G = \frac{\delta(\xi)}{\Delta\eta}, \qquad 0 \le \eta \le \Delta\eta \tag{3d}$$

$$G = 0, \qquad \Delta\eta < \eta \tag{3e}$$

The dimensionless temperature θ must be obtained from Eq. (3c) each time a temperature is desired in the numerical solution. In the present problem the density and specific heat are taken to be constant; thus, $R(\theta) = 1$ and $C(\theta) = 1$. The dimensionless boundary and initial conditions for the preceding problem are taken to be

$$Q_0 = Q_{abs} - Bi_0(\theta - \theta_{\infty,0}), \qquad \eta = 0, \qquad \xi > 0 \tag{4a}$$

$$Q_1 = Bi_1(\theta - \theta_{\infty,1}), \qquad \eta = 1 \qquad \xi > 0 \tag{4b}$$

$$\theta = 0, \qquad 0 \le \eta \le 1, \qquad \xi = 0 \tag{4c}$$

In solutions involving internal heat generation, no external heat flux is absorbed at the surface, i.e., $Q_{abs} = 0$. However, convection is assumed present at the boundaries and is related to the difference in temperatures between the surface and the ambient. In each of the cases considered, a Biot number of zero at the right surface implies an adiabatic boundary. Equations (4a–4c) can be written in terms of H by use of Eq. (3c). To form a complete mathematical set of equations for the hyperbolic problem [Eqs. (1) and (3a) or (3b)], additional boundary conditions and an additional initial condition are necessary. The boundary conditions used in the numerical analysis are obtained by requiring that energy conservation be satisfied at each boundary. Thus, the additional boundary and initial conditions are given by

$$\frac{\partial H}{\partial \xi} + \frac{\partial Q}{\partial \eta} = 0, \qquad \eta = 0, \qquad \xi > 0 \tag{4d}$$

$$\frac{\partial H}{\partial \xi} + \frac{\partial Q}{\partial \eta} = 0, \qquad \eta = 1, \qquad \xi > 0 \tag{4e}$$

$$Q = 0, \qquad 0 \le \eta \le 1, \qquad \xi = 0 \tag{4f}$$

In the present analysis three different cases are studied. The first involves a step to a constant applied surface heat flux Q_{abs}. In this case G is zero. The second case involves a pulse surface heat flux, where $Q_{abs} = 0$ for $\xi > \Delta\xi$, and G is again 0. The final case involves internal heat generation as defined by Eqs. (3d) and (3e) in which the surface heat flux $Q_{abs} = 0$.

Methods of Solution

MacCormack's Predictor-Corrector Method

When numerically analyzing the HHC equation via MacCormack's predictor-corrector method, it is convenient to solve the energy and flux equation as a system of first-order partial differential equations (PDEs) rather than to combine the two equations into a single second-order PDE. MacCormack's predictor-corrector scheme has successfully been used to model moving discontinuities in both fluid flow and heat transfer and is chosen for the present analysis. The scheme is a second-order-accurate, explicit predictor-corrector sequence for the integration of partial differential equations. To apply MacCormack's method to the HHC problem, Eqs. (1) and (3b) are written in vector form as

$$\frac{\partial E}{\partial \xi} + [A]\frac{\partial F}{\partial \eta} + S = 0 \tag{5a}$$

where

$$E = \begin{bmatrix} H \\ Q \end{bmatrix} \tag{5b}$$

$$F = \begin{bmatrix} Q \\ \theta \end{bmatrix} \tag{5c}$$

$$S = \begin{bmatrix} -G/2 \\ 2Q/\tau \end{bmatrix} \tag{5d}$$

$$[A] = \begin{bmatrix} 1 & 0 \\ 0 & K/\tau \end{bmatrix} \tag{5e}$$

Now Eqs. (5a–5e), together with the boundary and initial conditions, Eqs. (4a–4f), constitute the complete mathematical formulation of the non-Fourier problem.

Using MacComack's method, the finite-difference form of Eq. (5a) becomes[23]

Predictor:

$$\tilde{E}_i^{n+1} = E_i^n - \nu\left[A_i^n\right]\left[F_{i+1}^n - F_i^n\right] - \Delta\xi S_i^n \tag{6a}$$

Corrector:

$$E_i^{n+1} = \tfrac{1}{2}\left[E_i^n + \tilde{E}_i^n\right] - \tfrac{1}{2}\left\{\nu\left[\tilde{A}_i^{n+1}\right]\left[\tilde{F}_i^{n+1} - \tilde{F}_{i-1}^{n+1}\right] - \Delta\xi\tilde{S}_i^{n+1}\right\} \tag{6b}$$

where the subscript i denotes the grid points in the space domain, and the superscript tilde refers to the predicted value at time level $n+1$. The Courant number ν is defined as $\nu = \Delta\xi/\Delta\eta$. Note that in the preceding formulation forward differencing is used in the predictor, whereas backward differencing is used in the corrector. The use of first-order forward and backward differencing in the predictor and corrector results in a combined second-order-accurate central differenced scheme. After each predictor or corrector calculation, the temperature must be obtained from the enthalpy by use of Eq. (3c).

Transfinite Element Method

In this section we focus on the numerical solution of the HHC equations via the transfinite element method using specially tailored elements. A unique feature of the method presented herein for HHC lies not only in the hybrid nature of the method but also in the use of specially tailored elements for accurately predicting the propagating thermal disturbances. Briefly summarized, a principal advantage in the use of transfinite element formulations for HHC models is that the time parameter can be eliminated, thereby requiring the hybrid formulation of a steady type of problem. After dividing the physical domain of interest into elements appropriate for a given problem, the first step involves applying the selected transform (Laplace transform is employed in this paper) in time to the governing transient HHC equations. Once the type of elements and their interpolation functions have been selected, the finite element formulations in the transform domain are derived via classical Galerkin procedures. The system equations are assembled next following the usual procedures of finite element assembly and then solved in the transform domain itself. Through an appropriate numerical inversion technique, the solution response can then be obtained at desired times during the transient. Applicability of specially tailored hybrid transfinite formulations for problems relevant to non-Fourier effects has been presented by Tamma and Railkar.[18,19]

The selection of the interpolation functions is an important consideration for accurately predicting the propagation of the thermal wave front. Although this selection is arbitrary in the generalized transfinite element method, for the solutions presented in this paper, specially tailored elements are employed to yield accurate representations for the propagating thermal disturbance, as described in the following section.

The HHC models are analyzed by first discretizing the given domain Ω into finite elements. The discretized finite element equations are obtained by applying the selected transform with respect to time to the equations governing HHC with convection boundary conditions and then employing the classical Galerkin procedures.

Although, in a manner similar to the previous approach, the energy and flux equations could be used separately as a system of two first-order partial differential equations [i.e., Eqs. (1)

and (3b)], it is convenient via the present approach to combine the equations represented by Eqs. (1) and (3a). This facilitates selection of specially tailored elements as described later for the HHC models evaluated in the paper. As a consequence of combining Eqs. (1) and (3a), the following representation of the hyperbolic governing equation in the transformed Laplace domain is obtained as

$$\bar{L}(\bar{\theta}) + \bar{\Psi} = 0 \tag{7}$$

In Eq. (7) $\bar{\theta}$ is the nondimensionalized form of temperature in the transform domain, and $\bar{\Psi}$ contains the remaining terms such as internal heat source, etc., in the transform domain.

Specially Tailored Formulations

In general, polynomials are usually selected as interpolation functions to approximate the nondimensionalized temperature distributions within each element. However, for the class of one-dimensional HHC models evaluated in this paper, specially tailored elements are employed, since the governing equations in the transform domain permit such representations. Consider the transformed governing HHC [Eq. (7)] of nth order expressed as

$$a_n \frac{\partial^n \bar{\theta}}{\partial \eta^n} + a_{n-1} \frac{\partial^{n-1} \bar{\theta}}{\partial \eta^{n-1}} + \cdots + a_0 \bar{\theta} + \bar{\Psi} = 0 \tag{8}$$

The general solution to Eq. (8) can be represented in the form

$$\bar{\theta} \sum_{j=1}^{n} c_j \bar{\theta}_j(\eta) + \bar{\phi}(\eta) \tag{9}$$

where c_j, $j = 1$, n are arbitrary constants, $\bar{\theta}_j$ are typical functions associated with the homogeneous solution of Eq. (8), and $\bar{\phi}(\eta)$ is the particular solution. An element with n degrees of freedom can now be formulated based on the continuity requirements. And, since the differential equation has n constants of integration, the element interpolation functions are determined by imposing the conditions

$$\bar{\theta}(\eta_j) = \theta_j, \qquad j = 1,n \tag{10}$$

where η_j are the nodal coordinates, and $\bar{\theta}_j$ are the nodal values of the nondimensionalized temperatures. Imposing the conditions given by Eq. (10) into Eq. (9) leads to the nondimensionalized temperature approximation within each element as

$$\bar{\theta} = \sum_{\substack{j=1 \\ j \neq p}}^{N} N_j \bar{\theta}_j + N_p \bar{\theta}_p \tag{11}$$

where N_j are specially tailored interpolation functions, and $\bar{\theta}_j$ are the nodal values of the nondimensionalized temperature distributions within each element. The expression $N_p\bar{\theta}_p$ is an extra term that results due to the presence of the nonhomogeneous (or particular) part of the transformed governing equation. The resulting discretized equations for the n values of $\bar{\theta}$ in the domain Ω are obtained typically for each node i by equating to zero the integral over the domain Ω of the product of the weighting functions ($W_i = N_i$) and the residual in the transform domain. This results in the discretized equations represented as

$$\bar{K}\bar{\theta} = \bar{R} \tag{12}$$

where $\bar{K}$ has contributions from heat transfer due to conduction, the transformed form of the terms involving the relaxation parameter and capacitance (i.e., the contributions of the first- and second-order time derivatives), and convection. The heat load vector $\bar{R}$ has contributions from internal source (which also includes the additional relaxation term of the source arising due to non-Fourier effects), initial conditions, specified temperatures, and convection due to ambient conditions.

For the nondimensionalized form of the HHC equation, the following interpolation functions are proposed, assuming a two noded element as described by Tamma and Railkar[18]:

$$\bar{\theta} = \sum_{j=1}^{2} N_j \bar{\theta}_j + N_p \bar{\theta}_p \tag{13a}$$

where

$$N_1 = \sinh[\lambda(l_e - \eta)] / \sinh[\lambda l_e] \tag{13b}$$

$$N_2 = \sinh[\lambda \eta] / \sinh[\lambda l_e] \tag{13c}$$

$$N_p = 1 - N_1 - N_2 \tag{13d}$$

$$\lambda = (s/\beta)^{1/2} \tag{13e}$$

$$\beta = K/[RC(\tau s + 2)] \tag{13f}$$

It should be noted that the term $N_p\bar{\theta}_p$ is due to the presence of the nonhomogeneous part of the transformed hyperbolic differential equation, and $\bar{\theta}_p$ is known a priori and is a function of the initial conditions and the internal source term. The system of Eq. (12) is now solved in the transform domain, and through an appropriate numerical inversion technique,[24] the solution response is obtained at desired durations of the transient thermal response.

Comparative numerical results are discussed in the next section to validate the applicability of the methods of solution described in this paper for HHC.

Results and Discussion

In all of the following results, temperature distributions in a slab of dimensionless thickness $\eta = 1$ are shown as obtained using MacCormack's predictor-corrector method (solid lines) and the hybrid transfinite element method (open circles). The thermal properties and the thermal relaxation time were assumed constant. Thus, values of the dimensionless parameters representing the thermal conductivity, density, specific heat, and relaxation parameter were all taken to be unity. Convection heat transfer was assumed at the boundaries due to an ambient temperature of $\theta_{\infty,0} = \theta_{\infty,1} = 0.5$, and the initial temperature of the slab was assumed to be 0. The Biot number at each boundary was taken to be either 0.0 or 0.5 to study the effects of convection on the internal temperatures, The mechanism of thermal energy input to the slab was either a step surface heat flux, a pulse heat flux, or internal heat generation.

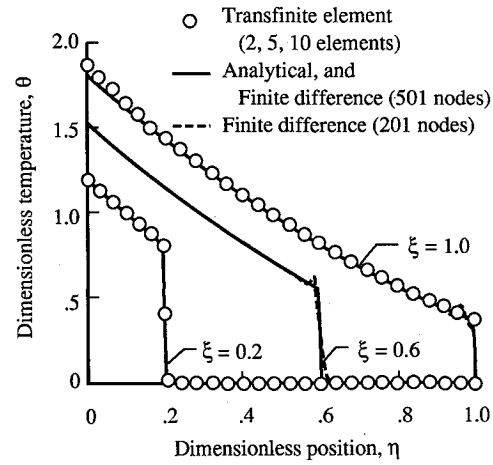

Fig. 2 Comparison of internal termperatures from finite-difference and transfinite element methods with a constant applied heat flux at $\eta=0$ for $\xi>0$ and an adibatic boundary at $\eta=1$.

Case 1: Step Surface Heat Flux

To verify both the accuracy and convergence of the numerical methods, Fig. 2 shows a comparison of the finite-difference and transfinite element solutions vs the analytical solution for a HHC problem with a constant applied heat flux of $Q_{abs} = 1$ (for $\xi > 0$) at the left boundary with no convection ($Bi_0 = 0$) and an adiabatic boundary at $\eta = 1$. The temperature distributions are shown at dimensionless times of $\xi = 0.2$, 0.6, and 1.0. The transfinite element solution (for 2, 5, and 10 elements) is shown vs the analytical solution at $\xi = 0.2$; the finite-difference solution (for both 201 and 501 nodes) is shown vs the analytical solution at $\xi = 0.6$; and the transfinite element and finite-difference solutions are all shown vs the analytical solution at $\xi = 1.0$. The use of shape functions based on the analytical solution in the transfinite element method results in an exact solution for linear problems regardless of the number of elements used. The finite-difference solution, however, is a function of the number of nodes. As can be seen at $\xi = 0.6$ and $\xi = 1.0$, the solutions with 501 nodes are indistinguishable from the analytical solution, though the solution with 201 nodes is not discontinuous at the thermal front. In addition, it is observed that the finite-difference (dashed line) and transfinite element (open circles) solutions are in excellent agreement with the analytical solution (solid lines), as both numerical solution techniques capture the thermal fronts with high resolution. The difference between the transfinite element and the analytical solution at the left

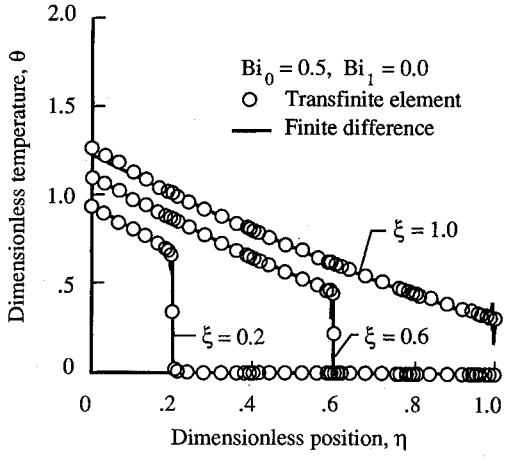

Fig. 3 Effect of convection on internal temperatures from finite-difference and transfinite element methods with a constant applied heat flux and convection at $\eta = 0$ for $\xi > 0$ and an adiabatic boundary at $\eta = 1$.

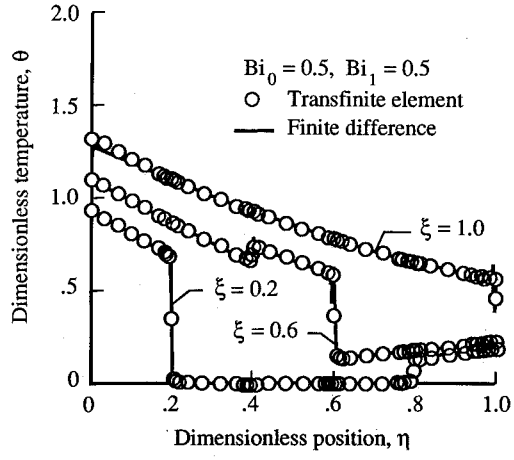

Fig. 4 Effect of convection on internal temperatures from finite-difference and transfinite element methods with a constant applied heat flux $\eta = 0$ for $\xi > 0$ and convection at both boundaries.

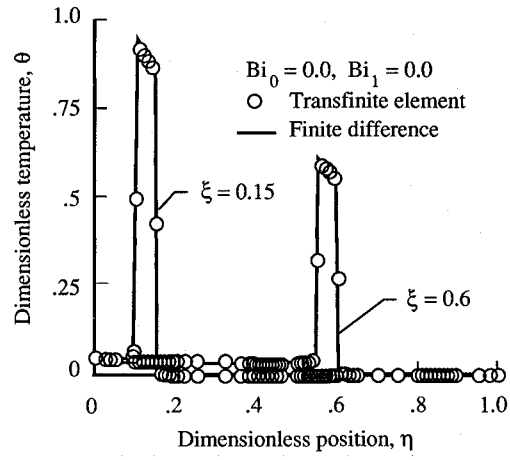

Fig. 5 Comparison of internal temperatures from finite-difference and transfinite element methods with pulse heating of duration $\Delta\xi = 0.05$, followed by an adiabatic boundary at $\eta = 0$ and an adiabatic boundary at $\eta = 1$.

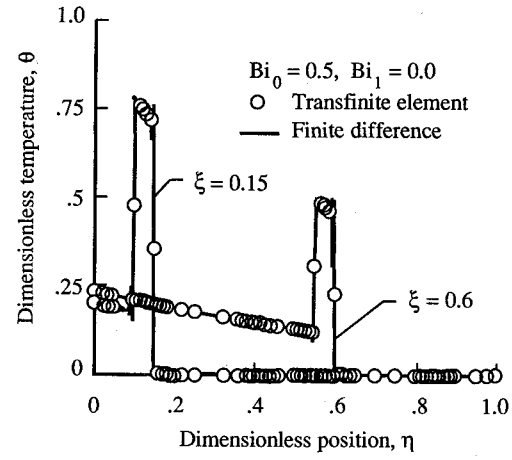

Fig. 6. Effect of convection on internal temperatures from finite-difference and transfinite element methods with pulse heating of duration $\Delta\xi = 0.05$ and convection at $\eta = 0$ and an adiabatic boundary at $\eta = 1$.

surface at $\xi = 1.0$ is due to the numerical inversion used to obtain the solution. In order to obtain an accurate, converged solution, the refined mesh of 501 nodes was used in all of the finite-difference solutions, whereas two elements used in the transfinite element solutions.

Figures 3 and 4 present solutions at the same time intervals with convection boundary conditions. In Fig. 3 convection is present at the left surface ($Bi_0 = 0.5$), and the right surface is adiabatic. The temperatures in Fig. 3 are lower than the corresponding curves in Fig. 2 due to the loss of energy from the left surface due to convection. In Fig. 4 the Biot number at both boundaries was taken to be 0.5 (i.e., $Bi_0 = Bi_1 = 0.5$). An interesting phenomenon is observed to occur when a wave front propagates from the right surface ($\eta = 1$) as well as from the left surface ($\eta = 0$). The wave front propagating from the right surface results from the convective heating of that surface. The wave front is of smaller magnitude (due to less applied thermal energy) but propagates at the same velocity (due to assumption of constant properties) as that originating from the left surface. At the center of the slab, the two thermal fronts meet and a summation effect is observed, which is a known property of linear hyperbolic systems of equations. This is noticed in the $\xi = 0.6$ solution, where the thermal front originating at $\eta = 0$ is observed to be added to the thermal front originating at $\eta = 1$. The region of summation is $0.4 \leq \eta \leq 0.6$, since both fronts have propagated into the medium a distance of $\eta = 0.6$. As stated by Taitel,[11] this summation effect may give unrealistically high temperatures

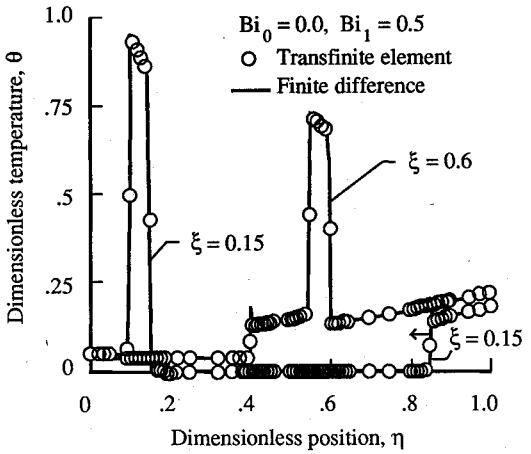

Fig. 7 Effect of convection on internal termperatures from finite-difference and transfinite element methods with pulse heating of duration $\Delta\xi = 0.05$ followed by an adiabatic boundary at $\eta = 0$ and convection at $\eta = 1$.

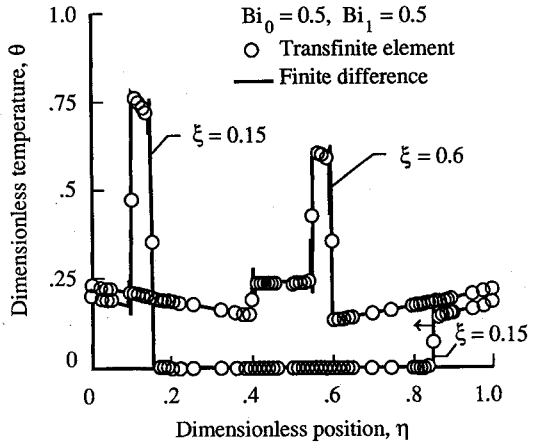

Fig. 8 Effect of convection on interal temepratures from finite-difference and transfinite element methods with pulse heating of duration $\Delta\xi = 0.05$ and convection at both boundaries.

when the interior temperatures are greater than the surface temperatures (due to the summation of the two thermal fronts). Thus, unrealistic aspects may be present in both the hyperbolic (excessively high temperatures due to summation) and parabolic (infinite propagation speed) models. However, this does not diminish the importance of the HHC equation for certain short time situations.

Case 2: Pulse Heat Flux

Figures 5–8 present solutions in which the slab is heated by a unit pulse heat flux of duration $\Delta\xi = 0.05$ at the left boundary. The temperature distributions are shown at dimensionless times $\xi = 0.15$ and 0.6. In each of Figs. 5–8 it is again observed that the finite-difference method and the transfinite element method are in excellent agreement. The slight differences occur because the transfinite element method does not exhibit the numerical oscillations that the finite-difference solution exhibits. The reason is that the transfinite element uses specially tailored elements. Temperatures within the slab for the case of no surface convection ($Bi_0 = 0$ and $Bi_1 = 0$) are shown in Fig. 5. It is noticed that the pulse propagates through the slab, maintaining its original pulse width, while shrinking in magnitude as it leaves energy in its wake. In Fig. 6 the magnitude of the pulse is less than in Fig. 5 due to the convective cooling at the left surface ($Bi_0 = 0.5$). During the heating period, $0 < \xi \leq 0.05$, the ambient conditions result in a cooling of the surface, whereas for $\xi > 0.05$, the ambient temperature results in convective heating of the surface. Convective heating at only the right surface ($Bi_1 = 0.5$) results in a continuous thermal front propagating from the right surface at the same speed as the pulse, but in the opposite direction, as shown by the arrow in Fig. 7. When the two fronts meet in the center of the slab, a summation of the temperatures is observed, as is the nature of phenomenon governed by hyperbolic equations. In Fig. 8, convection is present at both surfaces ($Bi_0 = 0.5$ and $Bi_1 = 0.5$), resulting in continuous heating both behind the pulse and at the right surface.

Case 3: Internal Heat Generation

The temperature distribution in a slab with internal generation (and $Q_{abs} = 0$) is shown in Figs. 9–11 at time $\xi = 0.3$. The heat generation is of magnitude $1/\Delta\eta$ in the region $0 \leq \eta \leq \Delta\eta$ at time $\xi = 0$, where $\Delta\eta = 0.02$. This results in a pulse propagating through the medium, similar to the pulse generated by a surface heat pulse. The location of the thermal front is at position $\eta = 0.32$, rather than $\eta = 0.3$, since the pulse was initially in the region $0 \leq \eta \leq 0.02$. It should be noted that in each of Figs. 9–11 the temperature scale extends below zero to show the spurious numerical spike in the finite-difference solution. In Fig. 9 convection is assumed at the left surface ($Bi_0 = 0.5$ and $Bi_1 = 0$), wherease in Fig. 10 convection is assumed at the right surface ($Bi_0 = 0$ and $Bi_1 = 0.5$), and in Fig. 11 convection is assumed at both surfaces ($Bi_0 = 0.5$ and $Bi_1 = 0.5$). Again, the agreement between the finite-difference and transfinite element solutions is quite good, though a numerical spike is observed in the finite-difference solution. It

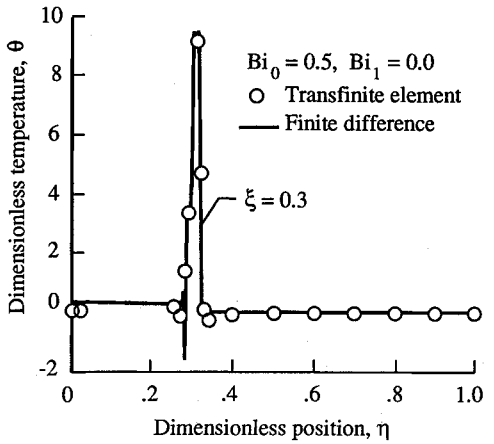

Fig. 9 Effect of convection on internal temperatures from finite-difference and transfinite element methods with a pulse internal generation and convection at $\eta = 0$ and an adiabatic boundary at $\eta = 1$.

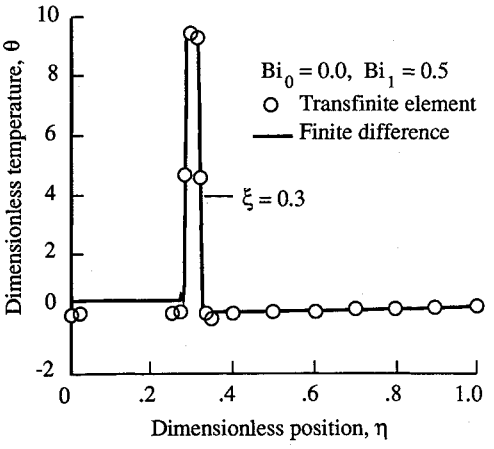

Fig. 10 Effect of convection on internal temperatures from finite-difference and transfinite element methods with a pulse internal generation and an adiabatic boundary at $\eta = 0$ and convection at $\eta = 1$.

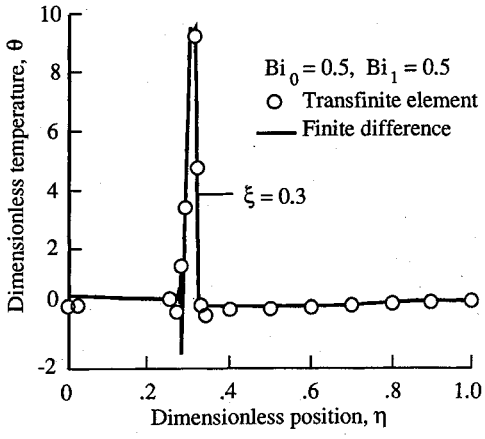

Fig. 11 Effect of convection on internal temperatures from finite-difference and transfinite element methods with a pulse internal generation and convection at both boundaries.

should be noted that any slight differences between the two methods at the left boundary is believed to be due to the differences in the time integration procedure of MacCormack's predictor-corrector method and the numerical inversion employed in the transfinite element formulations. In Fig. 9 convective heating at the left surface results in slightly higher temperatures behind the pulse than those observed in Fig. 10 (no convective heating at the left surface). Likewise, convective heating at the right surface in Fig. 10 results in slightly larger temperatures near the right surface than are observed in Fig. 9 (no convective heating at the right surface). In Figs. 9 and 11, where convection is present at the left surface, it is noticed that the trailing edge of the pulse is not vertical, in contrast to the square-wave-type pulse in Fig. 10 (no connection at the left surface). This wedge-shaped pulse (where the leading edge of the pulse remains vertical, but the trailing edge is sloped) is a result of convection at the surface where the pulse originated. As seen in Fig. 10, and as analytically predicted by Ref. 15, an internally generated pulse next to an adiabatic boundary maintains its square-wave nature as it propagates into the medium.

Concluding Remarks

This paper describes two methods of approach for analyzing HHC problems influenced by convection boundary conditions with various mechanisms of thermal energy input, i.e., step surface heat flux, pulse surface heat flux, and internal generation. The agreement of the finite-difference method and the transfinite element method validates the actual representation of the HHC problems with convection boundary conditions. It has been observed that convective heating alone results in a thermal front propagating through the medium. In addition, some interesting observations are noticed. For example, if an internal heat source pulse is introduced (as a square wave) without any convection effects, the propagating disturbance maintains the square-wave nature. However, if the pulse internal source is generated next to a convecting surface, the pulse shape is disturbed. That is, the propagating leading front is still vertical, whereas the trailing edge is slanted, resulting in an almost right triangular propagating pulse. No effect is observed on the pulse shape if convection is present at the right boundary since the convective heat flow must propagate through the slab before it effects the propagating thermal pulse.

Acknowledgment

The authors are pleased to acknowledge support of this research in part by the Thermal Structures Branch, NASA Langley Research Center, Hampton, VA.

References

[1]Nayfeh, A., and Nemat-Nasser, S., "Thermoelastic Waves in Solids with Thermal Relaxation," *Acta Mechanica,* Vol. 12, 1971, pp. 53–69.

[2]Torczynski, J. R., Gerthson, D., and Roesgen, T., "Schlieren Photography of Second Sound Shock Waves in Superfluid Helium," *Physics of Fluids,* Vol. 27, 1984, pp. 2418–2423.

[3]Ackerman, C. C., and Overton, W. C., Jr., "Second Sound in Solid Helium-3," *Physical Review Letters,* Vol. 22, No. 15, 1969, pp. 764–766.

[4]Hager, N. E., III, and Constable, J. H., "Heat Pulse Transmissions from Solid Floride into Helium I," *Journal of Low Temperature Physics,* Vol. 61, No. 5/6, 1985, pp. 455–470.

[5]Brorson, S. D., Fujimoto, J. G., and Ippen, E. P., "Femtosecond Electronic Heat-Transport Dynamics in Thin Gold Films," *Physical Review Letters,* Vol. 59, 1987, pp. 1962-1965.

[6]Kaushik, T. C., and Godwal, B. K., "Laser-driven Shock Pressure in Plane-layered CH_2-Pt Targets," *Physical Review A*, Vol. 36, No. 10, 1987, pp. 5095–5098.

[7]Chan, S. H., Low, M. J. D., and Mueller, W. K., "Hyperbolic Heat Conduction in Catalytic Supported Crystallites," *AIChE Journal,* Vol. 17, No. 6, 1971, pp. 1499–1501.

[8]Maxwell, J. C., "On the Dynamical Theory of Gases," *Philosophical Transactions of the Royal Society of London*, Vol. 157, 1867, p. 49–88.

[9]Vernotte, P., "Les Paradoxes de la Theorie Continue de l'equation de la Chaleur," *Comptes Rendus Hebdomadaires des Seances de l'Academie des Sciences,* Vol. 246, 1958, pp. 3154–3155.

[10]Gurtin, M. E., and Pipkin, A. C., "A General Theory of Heat Conduction with Finite Wave Speed," *Archives for Rational Mechanics Analysis,* Vol. 31, 1968, pp. 113–126.

[11]Taitel, Y., "On the Parabolic, Hyperbolic and Discrete Formulation of the Heat Conduction Equation," *International Journal of Heat and Mass Transfer*, Vol. 15, 1972, pp. 369–371.

[12]Berkovsky, B. M., and Bashtovoi, V. G., "The Finite Velocity of Heat Propagation from the Viewpoint of the Kinetic Theory," *International Journal of Heat and Mass Transfer,* Vol. 20, 1977, pp. 621–626.

[13]Maurer, M. J., and Thompson, H. A., "Non-Fourier Effects at High Flux," *Journal of Heat Transfer,* Vol. 95, 1973, pp. 284–286.

[14]Baumeister, K. J., and Hamill, T. D., "Hyperbolic Heat Conduction Equation—a Solution for the Semi-Infinite Body Problem," *Journal of Heat Transfer,* Vol. 91, 1969, pp. 543–548.

[15]Özisik, M. N., and Vick, B., "Propagation and Reflection of Thermal Waves in a Finite Medium," *International Journal of Heat and Mass Transfer,* Vol. 27, 1984, pp. 1845–1854.

[16]Wiggert, D. C., "Analysis of Early-Time Transient Heat Conduction by Method of Characteristics," *Journal of Heat Transfer,* Vol. 99, 1977, pp. 35–40.

[17]Glass, D. E., Özisik, M. N., McRae, D. S., and Vick, B., "On the Numerical Solution of Hyperbolic Heat Conduction," *Numerical Heat Transfer,* Vol. 8, 1985, pp. 497–504.

[18]Tamma, K. K., and Railkar, S. B., "Specially Tailored Transfinite Element Formulations for Hyperbolic Heat Conduction Involving Non-Fourier Effect is," *Numerical Heat Transfer,* Vol. 15(b), 1989, pp. 211–226.

[19]Tamma, K. K., and Railkar, S. B., "Evaluation of non-Fourier Stress Wave Distribution Via Tailored Hybrid Transfinite Element Formulations," AIAA Paper 89-1190, April 1989.

[20]Wu, C. Y., "Integral Equation Solution for Hyperbolic Heat Conduction with Surface Radiation," *International Communication on Heat and Mass Transfer*, Vol. 15, 1985, pp. 365–374.

[21]Glass, D. E., Özisik, M. N., and Vick, B., "Hyperbolic Heat Conduction with Surface Radiation," *International Journal of Heat and Mass Transfer,* Vol. 28, 1985, pp. 1823–1830.

[22]Glass, D. E., Özisik, M. N., and Vick, B., "Non-Fourier Effects on Transient Temperature Resulting From Periodic On-Off Heat Flux," *International Journal of Heat and Mass Transfer*, Vol. 30, 1987, pp. 1623–1631.

[23]Anderson, D. A., Tannehill, J. C., and Pletcher, R. H., *Computational Fluid Mechanics and Heat Transfer,* Hemisphere, Washington, DC, 1984, pp. 102–103.

[24]Durbin, F., "Numerical Inversion of Laplace Transforms: An Efficient Improvement to Dubner and Abate's Method," *Computer Journal*, Vol. 17, 1979, pp. 371–376.